Interrogating a single light-driven rotary molecular motor with force

Maxime Ledent,[1‡] Yohan Gisbert,[2‡] Damien Sluysmans,[1] R. Dean Astumian,[3] Ben L. Feringa,[2*] Anne-Sophie Duwez[1*]

[1] UR Molecular Systems, Department of Chemistry, University of Liège, Liège, Belgium
[2] Stratingh Institute for Chemistry, University of Groningen, Groningen, The Netherlands
[3] Department of Physics and Astronomy, The University of Maine, Orono, USA

‡These authors contributed equally to this work

* Correspondence and requests for materials should be addressed to A.-S.D. (asduwez@uliege.be, force spectroscopy experiments) or B.L.F. (b.l.feringa@rug.nl, synthesis)

Abstract

Inspired by Nature, where molecular motors are central to numerous life processes, chemists have developed a variety of artificial molecular machines[1–6], including rotative motors[7–9]. These motors generate continuous directional motion when driven by an energy input. Due to their tiny size, an order of magnitude smaller than their biological counterparts, most of the knowledge on their functioning was gained through bulk population studies, revealing averaged behaviour at the macroscopic scale. Crucial properties, such as the output force upon actuation, which is a key challenge towards future nanomechanical machines, could not be directly measured, and were extracted from theoretical or semiempirical calculations[10–12]. Single-molecule force spectroscopy has proven highly effective to uncover key energetic and mechanistic parameters[13–16], but has never been applied to synthetic rotative molecular motors, due to the extreme difficulty to probe processes at the 1-nanometer scale, while combining force measurements and the application of an external stimulus. Here, we developed distance-clamp experiments under UV-light irradiation to probe a single light-driven overcrowded-alkene rotary molecular motor at work. We applied mechanical loads to the motor and directly measured its operating force. The results also allowed the experimental validation of the principle of microscopic reversibility applied to light-driven motors, which had been theoretically predicted but never observed so far[17]. Quantitative information obtained here is crucial to establish future design principles for nanometer-scale devices capable of efficiently producing work and mechanical tasks.

Main text

Introduction

Taking inspiration from biological rotary motors such as the adenosine triphosphate (ATP) synthase[18] and the bacterial flagellar motor[19], chemists have long sought to synthesize analogous molecular machinery, able to undergo unidirectional rotation. The first synthetic unidirectional rotary molecular motor, based on the light-driven isomerization of an overcrowded alkene, was reported in 1999[7]. At the same time, a 120° directional rotation, using a chemical-fuelled triptycene-based molecular ratchet, was demonstrated[20]. Subsequently, chemical-driven unidirectional motors involving rotation around single bonds were demonstrated[21–24]. Directional rotation has also been realized in a number of systems, including light-driven imine motors[25], catenanes that undergo pulsed[26] or autonomous[27] chemically fuelled rotation of one macrocycle around another and hemithioindigo rotary motors[28].

Although much of the detailed understanding of how biological machines operate has been gleaned from direct force measurements made on single molecules with optical tweezers or atomic force microscopy (AFM)[13–15], none of the synthetic light-driven rotary motors, which are an order of magnitude smaller than their natural counterparts, were investigated by such techniques. With the exception of fluorescence measurements evidencing the unidirectional rotary motion of a light-driven motor at the single molecule level[29], only combinations of standard spectroscopic methods (NMR, UV-Vis, CD, etc.) addressing populations of synthetic light-driven motors have been used so far, preventing crucial information about their operation from being obtained. The single molecular scale indeed allows the detection of unique behaviours that are usually hidden in the averaged signal of a population of molecules. We previously described the use of AFM-based single-molecule force spectroscopy (SMFS) to gain crucial insights on linear molecular machines such as (oligo)rotaxanes[30–33], catenanes[34], and non-directional oscillating rotors[35], and envisioned that this technique could provide unprecedented knowledge on the functioning of rotary light-driven molecular motors. Here, we use AFM–based SMFS to probe a second–generation overcrowded alkene–based molecular motor at work. This motor can unidirectionally rotate under UV irradiation through two photoisomerization steps interspersed with two thermally–activated helix inversion steps (THI)[7], completing a 360° rotary cycle. We developed experiments combining the clamping of a single molecule during force measurements and *in-situ* UV irradiation. In 2002, Gaub and co-workers proposed an archetypal thought experiment combining the mechanical pulling of a light-responsive polymer based on molecular photoswitches and its irradiation in an optomechanical cycle[16]. Here, we go major steps further, by succeeding in realizing the unprecedented direct measurement of a molecular rotary motor at work under continuous light-

driven operation at the single-molecule scale. These measurements were performed using distance-clamp experiments, which allowed to directly probe the rotation of the motor and measure its operating force and energy landscape. The results were then used to experimentally demonstrate the microscopic reversibility principle applied to rotary molecular motors, which was theoretically postulated[17] but never experimentally verified.

Measuring the molecular motor at work

To enable the interfacing of the molecule with the AFM force spectroscopy setup, we designed a motor with a polyethylene glycol (PEG) chain on the rotor part and alkyne anchoring groups on the stator unit of second generation[9] light-powered molecular rotary motor (Fig.1a ; Supplementary section 1). The molecules were grafted through "*click*" Copper(I)-catalysed Alkyne-Azide Cycloaddition (CuAAC)[36] on an activated glass surface featuring pendant azide groups (Supplementary section 2). The PEG chain can physisorb onto the AFM tip and act as a connecting tether to track the rotor's motion. We previously showed that this approach, based on the physisorption of PEG tethers onto the tip, provides a strong and stable attachment of the molecule, adequate to obtain reliable data on the behaviour of the system grafted onto the surface[30,33–35,37–41].

To validate the possibility of carrying out force measurements on molecular motors attached to the surface, standard pulling experiments were carried out on the molecule without irradiation (See Methods). The AFM tip was brought into contact with the anchored motor-PEG substrate in *N,N*-dimethylformamide, allowing the PEG tether to adsorb onto the tip. The caught molecule was then stretched in a controlled manner by moving the tip away from the substrate at a fixed pulling rate, and the force–extension profiles were measured (Extended Data Fig. 1). The reoccurring single peak profiles with the expected range of extensions and persistence lengths[42], consistent with the structural parameters of the system, suggest that a single molecule was being stretched by the tip and confirms the experimental design suitability (Extended Data Fig. 2).

The single-molecule controlled distance-clamp (DC) experiments were then combined with optical excitation. Typically, after physisorption of the PEG chain onto the AFM tip, the molecule was extended to a constant distance (*i.e.* clamping distance) (see Methods), bringing the system under tension. Simultaneous constant UV irradiation (365 nm) through the glass surface (Extended Data Fig. 3) triggered the unidirectional rotation of the motor, resulting in aperiodical pulling on the tip through the PEG chain. This molecular motion is transduced to the tip-bearing cantilever, the resulting bending displacement being proportional to the force that is applied on the motor and against which the motor generates work. Figure 1b represents the rotation-triggered force modulation over time, showing the oscillation between two states, the relaxed and tensed states, with hopping phenomena taking place periodically (additional

DC curves are shown in Extended Data Fig. 4). A control curve, realized in the dark, is shown in Extended Data Fig. 5 and no hopping was detected.

Using transient absorption spectroscopy, we previously studied a similar second-generation motor design featuring an unfunctionalized rotor which was found to have a half-life time for the thermal helix inversion (THI) process of 38 ± 1 ns[36]. Thus, considering the timeframe of the present DC experiments and the lifetime of the observed tensed and relaxed states, the high-energy metastable states cannot be observed individually as their decay appears concomitant to the photoisomerization at this timescale. Moreover, the *E/Z* photoisomerization of the overcrowded alkene produces a large geometrical change, resulting in a high-amplitude motion (corresponding to the measured tip displacement, *vide infra*), whereas the subsequent THI process induces a low-amplitude geometric rearrangement. Both observed relaxed and tensed states thus correspond mostly to both stable states of the motor, with negligible contributions of the short-lived metastable isomers. As these experiments are performed at the single-molecule scale, the speed of the motor is not determined by the kinetically slower THI, as usually observed in bulk[9], but by a combination of the probability of the molecule to interact with a photon of the right energy under the experimental irradiation conditions, combined with the quantum yield of the motor, explaining the long lifetimes observed for both states. From these results, we can conclude that the continuous unidirectional rotation of the motor is taking place during these experiments.

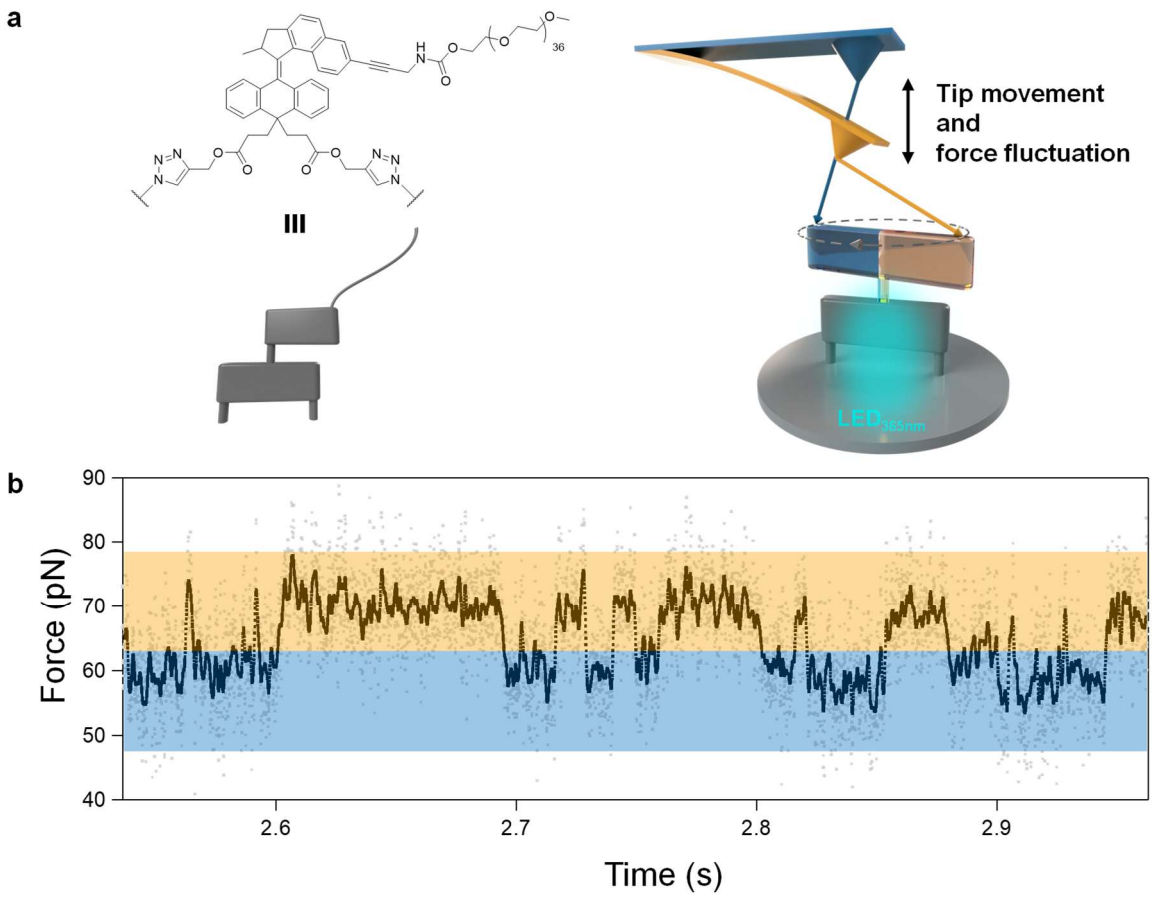

Fig. 1: Experimental setup and AFM response of the single molecule motor rotation. a, Chemical structure of the molecular motor and schematic representation (left). The system is irradiated by UV_{365nm} light during distance-clamp force spectroscopy experiments, leading to a hopping movement of the tip triggered by the motor rotation, switching from a relaxed (blue) to a tensed state (yellow) (right). **b**, Raw data (grey dots) and smoothed signal (black dots) showing the force measured by the cantilever over time upon motor rotation. The force fluctuates between the relaxed (blue band) and tensed (yellow band) states.

Estimation of the output force of the motor

Knowing the cantilever spring constant, the displacement of the tip during its hopping movement can be calculated for each hopping event observed during experiments according to Hooke's law (Extended Data table 1). While performing a 180° movement, the rotation diameter of the molecular rigid moiety has an approximative value of 2.0 nm (See Supplementary Section 3). The linear hopping movement operated by the tip leads to smaller values than the diameter of the rotor (Extended Data table 1). This can be explained by the random orientation of the molecule with respect to the tip. If the tip is perfectly aligned with the rotation plan of the motor, the recorded amplitude of the tip movement should be equal to the rotation diameter (Fig. 2a). When the tip moves away from the rotating plan of the motor, the linear actuation displacement decreases until it becomes almost null with the tip being aligned with the rotation axis (Fig. 2b).

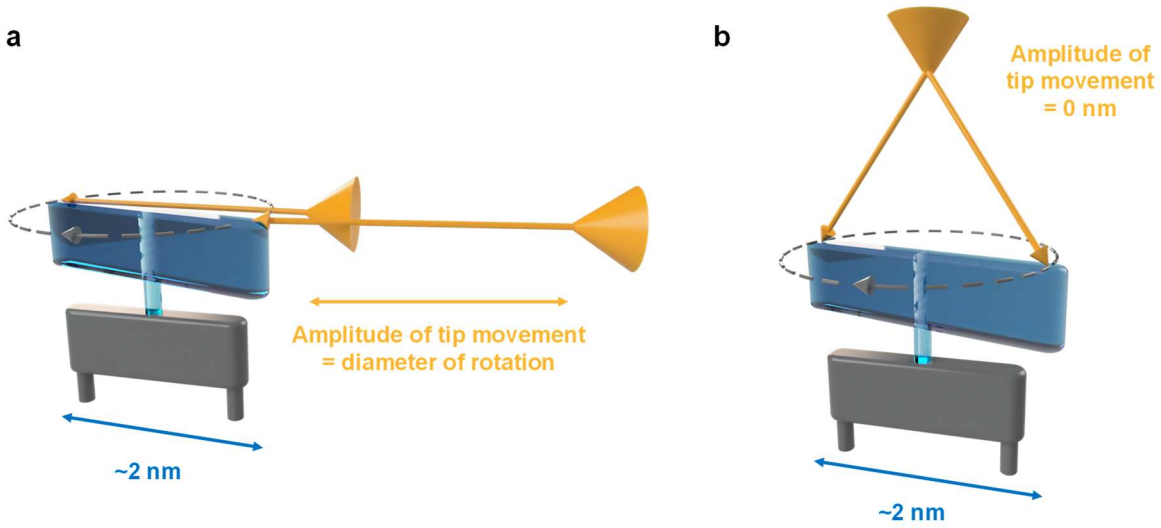

Fig. 2: Schematic of the position of the tip relative to the motor. a, Case where the tip is aligned with the rotation plan of the motor, leading to equal tip movement amplitude and rotation diameter. **b**, Case where the tip is perfectly aligned to the rotation axis of the motor, leading to a null movement of the tip during rotation.

The force exerted by the tip on the molecule can be decomposed into two components: one perpendicular to and the other aligned with the rotating plan. The latter will be called the 'effective force', as it is the actual force perceived by the motor while operating the rotation. The tip displacement can be used to recalculate the tilt angle of the molecule and estimate the effective force value (Calculations in Methods; Extended Data Fig. 6 and Table 2). The mean value of the effective force is 26 pN and can be considered as the force against which the motor can do work. As a comparison, Giuseppone *et al.* estimated a force of ~20 pN[11] for other second–generation molecular motors by means of energetic calculations associated with spectroscopic bulk experiments, which is in good agreement with the value obtained here by single-molecule measurements. Above this value, the motor rotation would be hampered. Even though the effective force value extracted from the experiments still allows the motor to rotate, the stall force value (*i.e.* the external force necessary to stop the motor rotation)[43] is close to the effective force. As a result, the effective force value measured here can be a reasonable estimation of the stall force for this second–generation molecular motor.

The mean effective force value has also been extracted from experiments carried on a gold surface using a specifically engineered analogue of the motor featuring thioether anchoring groups, and irradiated sideways using an optical fibre (instead of a LED through the sample). We obtained values in the same range (17 pN, Extended Data Table 2). The repeatability of measurements independently of the surface material, the grafting method, and the procedure for UV-irradiation, underlines the robustness of the method and further confirms the direct probing of the molecular motor rotation.

Determining the 1D energy landscape

The partition of the motor in the relaxed and tensed states can be established by measuring the occupancy frequency of each state in the hopping force range[44] (Fig. 3). The corresponding probability density function ($P(\theta)$) reflects the occupancy probability of the rotor in both states. Using the inverse Boltzmann method, the 1D energy landscape ($-kTln(P(\theta))$ of the motor can be reconstructed[45]. Since an external force is applied on the system, the landscape obtained by calculation of $-kTln(P(\theta))$ is related to the Gibbs free energy (ΔG) landscape of the motor by the expression $-kT\ln(P(\theta)) = \Delta G(\theta) + U_{\mathrm{AFM}}(\Delta d(\theta))$. For this reason, the more appropriate term "energy landscape" will be used here. The method has been used for every recorded hopping curve to calculate the mean values of the potential wells of the relaxed state (-0.428 kcal·mol^{-1}) and tensed state (-0.405 kcal·mol^{-1}). The nearly identical energy values indicate that the motor has equal probabilities to reach either stable configuration of the overcrowded alkene during the DC experiments. This equipartition is achieved by alternating from one state to the other, in a thermodynamically out-of-equilibrium process due to constant UV irradiation[46]. This demonstrates the ability of the motor to fulfil its motion trajectory via two stable states, as predicted in the well-established rotation mechanism of such motors[7,47].

The DC setup allows us to reach different external force values. While the distance between the tip and the surface is fixed, the tension in the system between them can vary, leading to different external forces applied on the motor. No correlation has been found between the external force exerted on the motor and the population occupancy in the 1D energy landscape. This can be explained by the small range of external forces values, decreasing drastically their impact on the rotational mechanism. In other words, the tension in the polymer linker is high enough to transduce the rotational motion to the tip but is too low to perturbate the rotation.

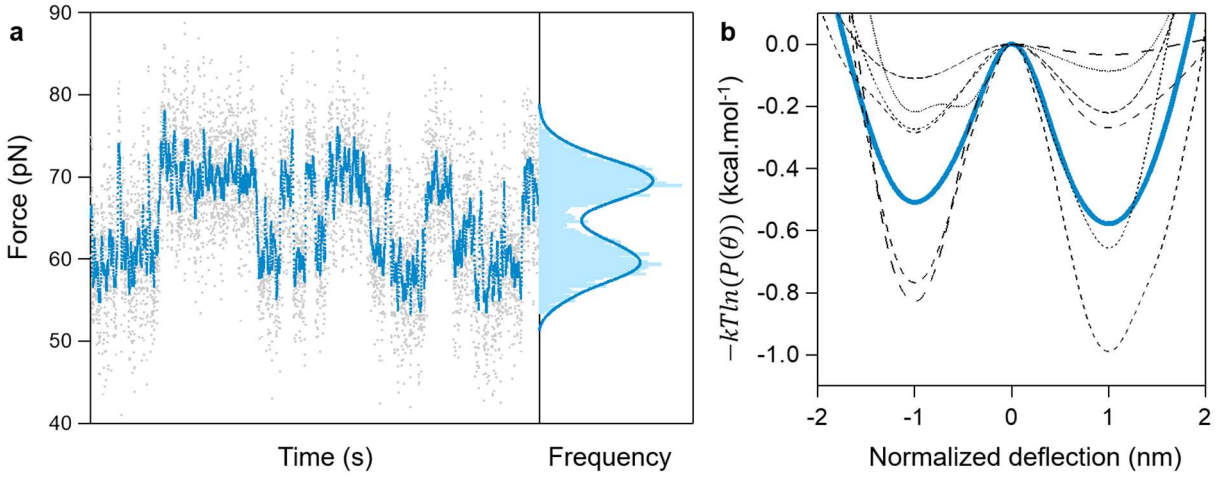

Fig. 3: Inverse Boltzmann method to determine the energy landscape. a, Raw data (grey dots) and smoothed signal (blue) of the force fluctuation. The associated histogram and probability density function of the relative occupancy is shown on the right panel. **b**, Plot of the energy landscape, $-kTln(P(\theta))$, vs the normalized tip deflection (blue line). The same calculations have been carried out on six other experimental datasets obtained with the same

experimental setup (dashed lines). The local maximum is used as the standard 0 value. The variations in population partitions does not depend on the external force and only depend on the time that the motor needs to successfully absorb a photon and trigger the photoisomerization. This mechanism remains stochastic at the single-molecular level and leads to variations in occupancy. The DC measurements have been repeated 6 times to consider this statistical effect and calculate mean energy values of the potential wells.

Verification of the microscopic reversibility principle applicability

Microscopic reversibility is a universal principle in chemistry and physics that governs the motion of molecules on a single energy surface –either the ground or the excited state. If a transition between a relaxed and tense state of a molecule occurs most probably by some pathway then the most probable transition from the tensed to the relaxed state must be the microscopic reverse of that path. As stated clearly in the IUPAC Gold Book, microscopic reversibility does not in general hold for light driven processes. However, as discussed in SI section 4, a corollary of microscopic reversibility –the direction independence of the last-touch-first-touch time– does hold, as shown in the present paper.

In the last decades, the direction independence of the last-touch-first-touch time has been hypothesized numerous times for out-of-equilibrium light fuelled systems, but has never been proven experimentally[17,48]. Implemented to the molecular motor, it states that the speed of the transition from the relaxed to the tensed state (quarter of a complete rotation) is the same as the speed of the transition in the other direction. It can be written as the core equation (Equation 1) of the corollary of microscopic reversibility[48,49] known as the last-touch-first-touch (LTFT) relation:

$$\tau_{\mathrm{LTFT}}(\mathrm{F}_{\mathrm{relaxed}} \rightarrow \mathrm{F}_{\mathrm{tensed}}) = \tau_{\mathrm{LTFT}}(\mathrm{F}_{\mathrm{tensed}} \rightarrow \mathrm{F}_{\mathrm{relaxed}})$$

where τ is the transition time needed by the motor to reach the mean force value of the tensed state ($\mathrm{F}_{\mathrm{tensed}}$) starting from the mean force value of the relaxed state ($\mathrm{F}_{\mathrm{relaxed}}$) and *vice versa,* where only trajectories that do not return to the starting force are included in the averaging. The rotation process of the molecular motor investigated here is based on a photoactivated isomerization and a thermally activated relaxation. While the latter is constrained by microscopic reversibility, the photoactivated step is described by Einstein equations[17] for absorption, stimulated emission and spontaneous emission of light. Nevertheless, in our experimental setup providing sufficiently bright conditions, the ratio of transition rate constants between the ground state and the excited state of the motor is unity (see Supplementary Section 4 for detailed equations). As a result, the principle of microscopic reversibility remains valid in the case of synthetic molecular motors[48,50], but has never been demonstrated experimentally so far. We have used Equation 1 to assess the applicability of microscopic reversibility to light-driven molecular motors.

Practically, on the force *vs* time plot (Fig. 4), the number of data points between the last data point in one state and the first data point reaching the other state were counted[48,49]. To study the impact of the external force on transition times, the analysis has been performed on 7 independent experiments. In all cases, the histogram superimposition of the number of data points recorded for both directions shows a high similarity with coincident PDF maximum value, regardless of the force applied on the rotor (Extended Data Fig. 7, Extended Data Table 3). This observation is consistent with Equation 1, which is independent of the external force due to the low Reynolds number of the surrounding environment. Consequently, as predicted by theory, the symmetry of the LTFT relation derived from microscopic reversibility remarkably applies to our experimental setup and remains valid for light-driven molecular motors.

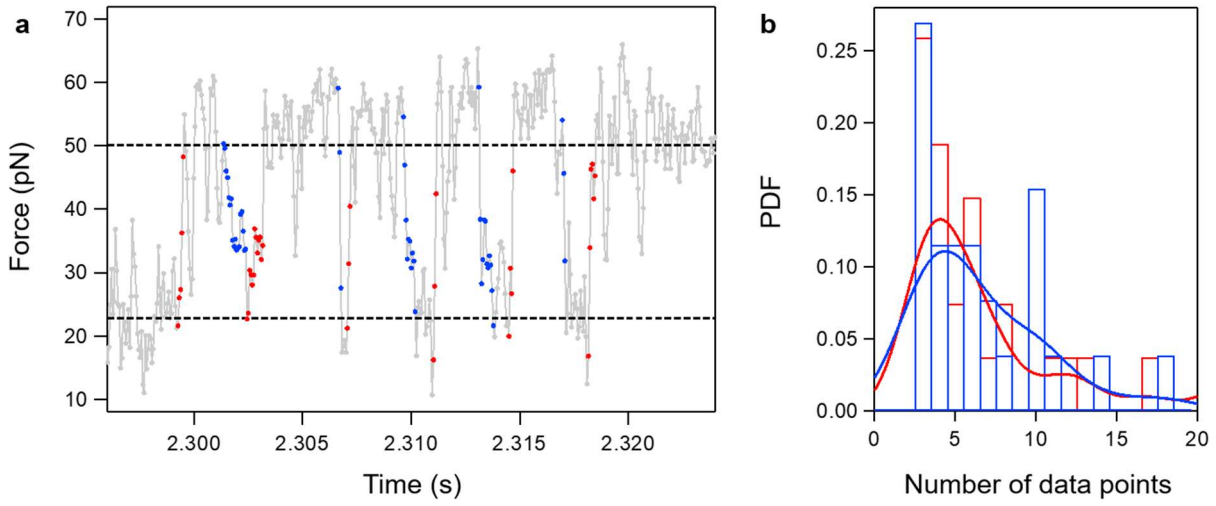

Fig. 4: LTFT analysis. a, Raw data (grey dots) and the number of data points needed to reach the tensed state from the relaxed state (red) and to reach the relaxed state from the tensed state (blue). The force values assigned to relaxed and tensed state (dashed lines) are extracted from the mean value of the gaussian deconvolution of the relative occupancy. **b**, Respective histograms and PDF, showing a high correspondence between both trajectories.

Conclusion

Over the past 25 years, light-driven molecular motors have progressed from fundamental scientific curiosities to versatile actuators with applications across diverse domains[8]. Despite this remarkable advancement, a key parameter, the force output of these synthetic molecular motors at the single-molecule level, remained unmeasured, representing a significant gap in our understanding of the functional capabilities of these molecular machines. Here, we developed SMFS-based distance clamp experiments combined with UV irradiation to shed light on the operation of an overcrowded-alkene-based rotary motor at the single-molecule scale. Clamping the motor between a surface and the AFM tip under constant UV irradiation enabled to directly probe the rotation, as the tip hops between two states during the high-

amplitude photoisomerization of the overcrowded alkene. We directly measured the force against which the motor can generate work, which was found to be 26 pN, in good agreement with previous estimations obtained from theoretical or semi-empirical calculations for other light-driven overcrowded-alkene-based motors[10–12]. A thorough statistical analysis of the data demonstrated a key result derived from the principle of microscopic reversibility, *i.e.*, that the last-touch first-touch times for two forces is independent of direction for (synthetic) light-driven molecular motors, which has been previously assumed but never proved through experiment. These fundamental results pave the way for the development of molecular motors with enhanced properties, unlocking applications across various fields. Until now, optimizing the force output of molecular motors to enable the transport of larger cargos or to amplify the work resulting from their collective motion at the molecular scale, often transferred across length-scales, has remained largely unexplored, primarily due to the inability to measure their output force. This study addresses that critical limitation, laying the groundwork for future advancements in the design and functionality of synthetic molecular motors.

Main references

1. Bissell, R. A., Córdova, E., Kaifer, A. E. & Stoddart, J. F. A chemically and electrochemically switchable molecular shuttle. *Nature* **369**, 133–137 (1994).
2. Dietrich-Buchecker, C. O., Sauvage, J. P. & Kintzinger, J. P. Une nouvelle famille de molecules : les metallo-catenanes. *Tetrahedron Lett.* **24**, 5095–5098 (1983).
3. Corra, S., Bakić, M. T., Groppi, J., Baroncini, M., Silvi, S., Penocchio, E., Esposito, M. & Credi, A. Kinetic and energetic insights into the dissipative non-equilibrium operation of an autonomous light-powered supramolecular pump. *Nat. Nanotechnol.* **17**, 746–751 (2022).
4. Kassem, S., Van Leeuwen, T., Lubbe, A. S., Wilson, M. R., Feringa, B. L. & Leigh, D. A. Artificial molecular motors. *Chem. Soc. Rev.* **46**, 2592–2621 (2017).
5. Kinbara, K. & Aida, T. Toward Intelligent Molecular Machines: Directed Motions of Biological and Artificial Molecules and Assemblies. *Chem. Rev.* **105**, 1377–1400 (2005).
6. Erbas-Cakmak, S., Leigh, D. A., McTernan, C. T. & Nussbaumer, A. L. Artificial Molecular Machines. *Chem. Rev.* **115**, 10081–10206 (2015).
7. Koumura, N., Zijlstra, R. W. J., van Delden, R. A., Harada, N. & Feringa, B. L. Light-driven monodirectional molecular rotor. *Nature* **401**, 152–155 (1999).
8. García-López, V., Liu, D. & Tour, J. M. Light-Activated Organic Molecular Motors and Their Applications. *Chem. Rev.* **120**, 79–124 (2020).
9. Pooler, D. R. S., Lubbe, A. S., Crespi, S. & Feringa, B. L. Designing light-driven rotary molecular motors. *Chem. Sci.* **12**, 14964–14986 (2021).
10. Li, Q., Fuks, G., Moulin, E., Maaloum, M., Rawiso, M., Kulic, I., Foy, J. T. & Giuseppone, N. Macroscopic contraction of a gel induced by the integrated motion of light-driven molecular motors. *Nat. Nanotechnol.* **10**, 161–165 (2015).
11. Gao, C., Vargas Jentzsch, A., Moulin, E. & Giuseppone, N. Light-Driven Molecular Whirligig. *J. Am. Chem. Soc.* **144**, 9845–9852 (2022).
12. Amano, S., Esposito, M., Kreidt, E., Leigh, D. A., Penocchio, E. & Roberts, B. M. W. Insights from an information thermodynamics analysis of a synthetic molecular motor. *Nat. Chem.* **14**, 530–537 (2022).
13. Bustamante, C., Chemla, Y. R., Forde, N. R. & Izhaky, D. Mechanical Processes in Biochemistry. *Annu. Rev. Biochem.* **73**, 705–748 (2004).
14. Pilizota, T., Sowa, Y. & Berry, R. M. Single-Molecule Studies of Rotary Molecular Motors. in *Handbook of Single-Molecule Biophysics* 183–216 (Springer US, 2009). doi:10.1007/978-0-387-76497-9_7.
15. Bustamante, C. Molecular machines one molecule at a time. *Protein Sci.* **26**, 1245–1248 (2017).
16. Hugel, T., Holland, N. B., Cattani, A., Moroder, L., Seitz, M. & Gaub, H. E. Single-Molecule Optomechanical Cycle. *Science* **296**, 1103–1106 (2002).
17. Astumian, R. D. Optical vs. chemical driving for molecular machines. *Faraday Discuss.* **195**, 583–597 (2016).
18. Boyer, P. D. The ATP synthase—a splendid molecular machine. *Annu. Rev. Biochem.* **66**, 717–749 (1997).
19. Sowa, Y., Rowe, A. D., Leake, M. C., Yakushi, T., Homma, M., Ishijima, A. & Berry, R. M. Direct observation of steps in rotation of the bacterial flagellar motor. *Nature* **437**, 916–919 (2005).
20. Kelly T.R., De Silva H. & Silva R.A. Unidirectional rotary motion in a molecular system. *Nature* **401**, 150–152 (1999).
21. Fletcher, S. P., Dumur, F., Pollard, M. M. & Feringa, B. L. A reversible, unidirectional molecular rotary motor driven by chemical energy. *Science* **310**, 80–82 (2005).
22. Collins, B. S. L., Kistemaker, J. C. M., Otten, E. & Feringa, B. L. A chemically powered unidirectional rotary molecular motor based on a palladium redox cycle. *Nat. Chem.* **8**, 860–866 (2016).
23. Zhang, Y., Chang, Z., Zhao, H., Crespi, S., Feringa, B. L. & Zhao, D. A chemically driven rotary molecular motor based on reversible lactone formation with perfect unidirectionality. *Chem* **6**, 2420–2429 (2020).
24. Borsley, S., Kreidt, E., Leigh, D. A. & Roberts, B. M. W. Autonomous fuelled directional rotation about a covalent single bond. *Nature* **604**, 80–85 (2022).
25. Greb, L. & Lehn, J.-M. Light-Driven Molecular Motors: Imines as Four-Step or Two-Step Unidirectional Rotors. *J. Am. Chem. Soc.* **136**, 13114–13117 (2014).
26. Erbas-Cakmak, S. Fielden, S. D. P., Karaca, U., Leigh, D. A., McTernan, C. T., Tetlow, D. J. & Wilson, M. R. Rotary and linear molecular motors driven by pulses of a chemical fuel. *Science* **358**, 340–343 (2017).

27. Wilson, M. R., Solà, J., Carlone, A., Goldup, S. M., Lebrasseur, N. & Leigh, D. A. An autonomous chemically fuelled small-molecule motor. *Nature* **534**, 235–240 (2016).
28. Bach, N. N., Josef, V., Maid, H. & Dube, H. Active Mechanical Threading by a Molecular Motor. *Angew. Chemie* **61**, 1–8 (2022).
29. Krajnik, B., Chen, J., Watson, M. A., Cockroft, S. L., Feringa, B. L. & Hofkens, J. Defocused Imaging of UV-Driven Surface-Bound Molecular Motors. *J. Am. Chem. Soc.* **139**, 7156–7159 (2017).
30. Lussis, P., Svaldo-Lanero, T., Bertocco, A., Fustin, C.-A., Leigh, D. A. & Duwez, A.-S. A single synthetic small molecule that generates force against a load. *Nat. Nanotechnol.* **6**, 553–557 (2011).
31. Sluysmans, D., Hubert, S., Bruns, C. J., Zhu, Z., Stoddart, J. F. & Duwez, A.-S. Synthetic oligorotaxanes exert high forces when folding under mechanical load. *Nat. Nanotechnol.* **13**, 209–213 (2018).
32. Sluysmans, D., Devaux, F., Bruns, C. J., Stoddart, J. F. & Duwez, A.-S. Dynamic force spectroscopy of synthetic oligorotaxane foldamers. *Proc. Natl. Acad. Sci.* **115**, 9362–9366 (2018).
33. Sluysmans, D., Lussis, P., Fustin, C.-A., Bertocco, A., Leigh, D. A. & Duwez, A.-S. Real-Time Fluctuations in Single-Molecule Rotaxane Experiments Reveal an Intermediate Weak Binding State during Shuttling. *J. Am. Chem. Soc.* **143**, 2348–2352 (2021).
34. Van Quaethem, A., Lussis, P., Leigh, D. A., Duwez, A.-S. & Fustin, C.-A. Probing the mobility of catenane rings in single molecules. *Chem. Sci.* **5**, 1449 (2014).
35. Li, X., Gisbert, Y., Ledent, M., Sluysmans, D., Rapenne, G., Kammerer, C. & Duwez, A.-S. Probing the free rotary oscillations around a single ruthenium atom in an organometallic complex. (2023) doi:10.26434/chemrxiv-2023-mgq5f-v3.
36. Vachon, J., Carroll, G. T., Pollard, M. M., Mes, E. M., Brouwer, A. M. & Feringa, B. L. An ultrafast surface-bound photo-active molecular motor. *Photochem. Photobiol. Sci.* **13**, 241–246 (2014).
37. Sluysmans, D., Zhang, L., Li, X., Garci, A., Stoddart, J. F. & Duwez, A.-S. Viologen Tweezers to Probe the Force of Individual Donor–Acceptor π-Interactions. *J. Am. Chem. Soc.* **142**, 21153–21159 (2020).
38. Sluysmans, D., Willet, N., Thevenot, J., Lecommandoux, S. & Duwez, A.-S. Single-molecule mechanical unfolding experiments reveal a critical length for the formation of α-helices in peptides. *Nanoscale Horizons* **5**, 671–678 (2020).
39. Devaux, F., Li, X., Sluysmans, D., Maurizot, V., Bakalis, E., Zerbetto, F., Huc, I. & Duwez, A.-S. Single-molecule mechanics of synthetic aromatic amide helices: Ultrafast and robust non-dissipative winding. *Chem* **7**, 1333–1346 (2021).
40. Calvaresi, M., Duwez, A.-S., Leigh, D. A., Sluysmans, D., Song, Y., Zerbetto, F. & Zhang, L. Mechanical tightening of a synthetic molecular knot. *Chem* **9**, 65–75 (2023).
41. Asano, M., Sluysmans, D., Willet, N., Bonduelle, C., Lecommandoux, S. & Duwez, A.-S. Single-molecule force spectroscopy shows that side chain interactions govern the mechanochemical response of polypeptide α-helices and prevent the formation of β-sheets. *RSC Mechanochemistry* **2**, 37–44 (2025).
42. Flory, P. J. & Mark, J. E. The configuration of the polyoxymethylene chain. *Die Makromol. Chemie* **75**, 11–21 (1964).
43. Ito, K. I., Sato, Y. & Toyabe, S. Design of artificial molecular motor inheriting directionality and scalability. *Biophys. J.* **123**, 858–866 (2024).
44. Jacobson, D. R. & Perkins, T. T. Quantifying a light-induced energetic change in bacteriorhodopsin by force spectroscopy. *Proc. Natl. Acad. Sci.* **121**, 2017 (2024).
45. Woodside, M. T., Anthony, P. C., Behnke-Parks, W. M., Larizadeh, K., Herschlag, D. & Block, S. M. Direct Measurement of the Full, Sequence-Dependent Folding Landscape of a Nucleic Acid. *Science* **314**, 1001–1004 (2006).
46. Astumian, R. D. Kinetic Asymmetry and Directionality of Nonequilibrium Molecular Systems. *Angew. Chemie Int. Ed.* **63**, (2024).
47. Browne, W. R. & Feringa, B. L. Making molecular machines work. *Nat. Nanotechnol.* **1**, 25–35 (2006).
48. Nicolás-García, T., Martín Sabanés, N., Bocanegra, R., Astumian, R. D., Pérez, E. M. & Ibarra, B. Transition-path times of individual molecular shuttles under mechanical equilibrium show symmetry. *Chem* **11**, 102410 (2025).
49. Bier, M., Derényi, I., Kostur, M. & Astumian, R. D. Intrawell relaxation of overdamped Brownian particles. *Phys. Rev. E* **59**, 6422–6432 (1999).
50. Astumian, R. D. Stochastically pumped adaptation and directional motion of molecular machines. *Proc. Natl. Acad. Sci.* **115**, 9405–9413 (2018).

Methods

AFM

SMFS experiments. SMFS experiments were carried on a MFP3D Origin+ (Asylum Research, Oxford Instruments) using HQ:CSC38/Al BS cantilevers (MikroMasch) with a nominal spring constant of ~0.03 $N.m^{-1}$. Prior to the experiments, the cantilevers were calibrated upon thermal method in air (Sader method) in order to determine the exact spring constant *k*. Grafted surfaces were placed in the fluid cell and immersed in anhydrous and filtered DMF. The cantilever was then immerged in the fluid cell away from the surface for 1h before the SMFS measurements to allow the system to equilibrate.

To ensure that the molecular motors were successfully grafted, standard approach and retraction cycles were realized with a tip velocity of 200 $nm.s^{-1}$. During approaching step, the tip is pushed toward the surface up to a force of 500 pN. Then, the tip is retracted to 100 nm away from the surface to ensure full molecular extension followed by desorption between each cycle. Raw deflection versus piezo–movement curves were transformed using Hooke's law:

$$F = -kx = -k(z - d)$$

with *F* the force experienced by the molecule, *k* the spring constant of the cantilever determined by Sader's method, *x* the cantilever deflection, *z* the piezo–movement and *d* the tip–substrate distance.

For the clamping experiments, 3 steps are needed. First, during the approaching step, the tip is pushed toward the surface up to a force of 500 pN. Then, a dwell time of 1 second is necessary to favour strong bonding between the polymer tether and the tip, allowing a long clamping time. Afterwards, the tip is retracted at a velocity of 200 $nm.s^{-1}$ to 10 nm from the surface for 3 seconds. Finally, the tip is approached toward the surface up to a force of 500 pN, then retracted to 100 nm at a velocity of 200 $nm.s^{-1}$ to complete the cycle. For experiments under irradiation, the surfaces were continuously irradiated with UV light using a LED placed bellow the glass surface (M365L3, Thorlabs) (Extended Data Figure 3).

Approach–retraction experiments analysis. Raw force versus piezo–movement curves were sorted using a homemade routine on the IgorPro software. Only experiments showing an occurrence of ~5% of events (*i.e.* stretching of a polymer chain) over the total number of approach–retraction cycles were kept as it comforts the single molecular level of the experiment[51].

Selected curves were analysed using a homemade routine allowing curves transformation, force–distance measurements and mathematical fitting. For all curves, the distance of the rupture of the link between the PEG linker and the tip was measured to build histograms. Automatic mathematical fit of curves applying the worm–like chain (WLC)[52] model was used in

the entropic region of curves (between 0 and 100pN). The WLC equation can be formulated as following:

$$F(D) = \frac{k_B T}{l_p}\left[\frac{D}{L} + \frac{1}{4(1-\frac{D}{L})^2} - \frac{1}{4}\right]$$

Were k_B is the Boltzmann constant and T the temperature. In our case, the persistence length (l_p) and the contour length (L) are the varying parameters of the curve fitting.

Histograms of distances, and l_p were constructed using IgorPro. Probability density function (PDF) were obtained by fitting the data by a Kernel smoothing function (N = 1000 points) with MatLab (MathWorks) and raw data were fitted using the Gaussian mixture model (GMM) in MatLab (MathWorks), i.e., a weighted sum of M components (i = 1, 2, 3) Gaussian densities as given by:

$$P(x|\lambda) = \sum_{i=1}^{M} p_i G(x|\mu_i, \sigma_i)$$

where x is the vector of the observable, $G(x|\mu_i, \sigma_i)$ is the normalized Gaussian component with mean μ_i and variance σ_i, and p_i is the weight of the i^{th} component. The weights satisfy the normalization condition $\sum_{i=1}^{M} p_i = 1$, and λ represents the set of all the parameters $\lambda = \{p_i, \mu_i, \sigma_i\}$ for i=1,2 or 3.

Each population is given with its 95% confidence interval estimated as $\pm 1.96\sqrt{\sigma^2/(p_i N)}$ where σ^2 is the estimated variance of the i^{th} component while $p_i N$ represents the effective size of the population.

Distance clamp experiments analysis. Raw force versus time curves were analysed using a homemade routine with the IgorPro software. Only the hopping zones of the clamping phase of curves were kept for further analysis.
Histograms of the fluctuating force were constructed in IgorPro and PDF were obtained with MatLab as described in the previous section. Then, PDF are deconvoluted into two gaussian curves were the two mean force values were taken as mean value of the relaxed and tensed states of the motor. In some cases, a small tip movement amplitude and a high cantilever spring constant can mask both populations into a broad peak. To extract the mean force values, the signal can be smoothed using a box size of 100.

The inverse Boltzmann method was realized according to reference 45. The probability density function PDF is used to construct the energy profile given by:

$$Energy = -k_B T ln(P(\theta))$$

Were k_B is the Boltzmann constant and T is the temperature. The resulting energy value was converted in kcal.mol^{-1} for representation.

Effective force calculation

As shown in Extended fig. 6, the cosine of the stretching angle has been taken to calculate the force component parallel to the rotating motion. To calculate the stretching angle from the tip movement amplitude *(*Δtip), the motion amplitude should vary between 0 and ~2 nm, being approximately the rotor diameter. The stretching angle can therefore be extracted according the equation:

$$\alpha = (90 - \Delta tip \times 45)$$

From there, the effective force can be calculated using the following equation:

$$effective\ force = external\ force\ \times cos(\alpha)$$

An observed Δtip of 2 nm would give a stretching angle of 0°, where the effective force is perfectly aligned to the rotation and a theoretical Δtip of 0 nm would result in a null value of the effective force as the external force is totally perpendicular to the rotation movement.

Experiments on gold surfaces

Experiments were also conducted on the motor grafted on gold substrates using thioether anchors[53,54] (See Supplementary Section 1 and 2). In this case, the sample is continuously irradiated sideways using an optical fibre, immersed in the fluid cell, with UV-light (M365L3, Thorlabs). Using the same distance clamp routine, hopping movements were also observed and have been reported in Extended Data Fig. 2 and 4. For clarity, the results exposed in the main text only detail the analysis of the molecular motor grafted on glass.

Methods references

51. Johnson, K. C. & Thomas, W. E. How Do We Know when Single-Molecule Force Spectroscopy Really Tests Single Bonds? *Biophys. J.* **114**, 2032–2039 (2018).
52. Giannotti, M. I. & Vancso, G. J. Interrogation of Single Synthetic Polymer Chains and Polysaccharides by AFM-Based Force Spectroscopy. *ChemPhysChem* **8**, 2290–2307 (2007).
53. van Delden, R. A., ter Wiel, M. K. J., Pollard, M. M., Vicario, J., Koumura, N. & Feringa, B. L. Unidirectional molecular motor on a gold surface. *Nature* **437**, 1337–1340 (2005).
54. Carroll, G. T., Pollard, M. M., van Delden, R. & Feringa, B. L. Controlled rotary motion of light-driven molecular motors assembled on a gold film. *Chem. Sci.* **1**, 97-101 (2010).

Acknowledgments

This work was supported by the European Research Council (ERC Advanced Grant 101054338, A.-S.D.), the F.R.S.-FNRS (CDR J.0074.22, A.-S.D.), the Netherlands Organization for Scientific Research (B.L.F.), the Royal Netherlands Academy of Arts and Sciences (B.L.F.), the Dutch Ministry of Education, Culture, and Science (Bonus Incentive Scheme and Gravitation Program 024.001.035 to B.L.F.), the European Union under the Marie Skłodowska-Curie actions individual fellowship n°101060079 (Y.G.).

Author contributions

A.-S.D., M.L., Y.G., and B.L.F. designed the experiments. Y.G. carried out the chemical synthesis and characterization studies. M.L. performed the AFM experiments and M.L. and D.S. analyzed the data. R.D.A. helped with the analysis of data for the microscopic reversibility principle. A.-S.D. and B.L.F. directed the research. M.L., Y.G. and A-S.D. wrote the paper. All the authors discussed the results and commented on the manuscript.

Competing interests

The authors declare no competing interests.

Materials & Correspondence

Correspondence and requests for materials should be addressed to A.-S.D. (asduwez@uliege.be, force spectroscopy experiments) or B.L.F. (b.l.feringa@rug.nl, synthesis)

Additional information

See Supplementary Information for detailed synthesis of molecular motors, grafting procedures, computational details, theoretical considerations for the applicability of microscopic reversibility.

Data availability

The data that support the findings of this study are available from the corresponding authors upon reasonable request.

Extended data figures

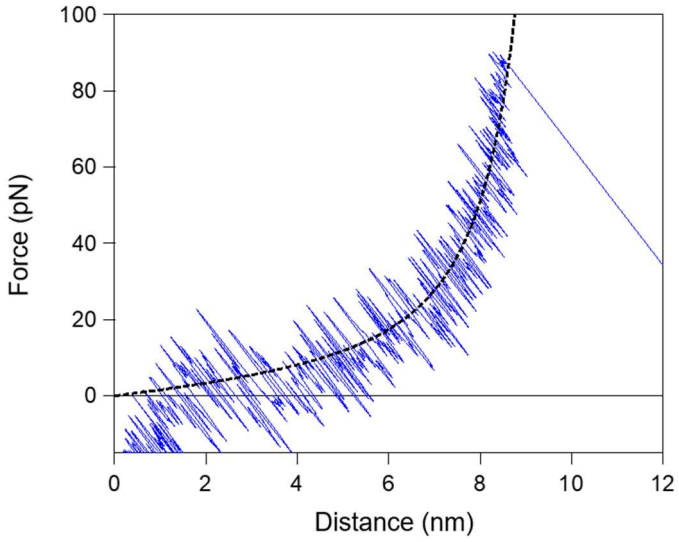

Extended Data Fig. 1: Force-extension curve obtained during a standard pulling experiment. The stretching of a single molecular motor leads to a typical force-extension curve (blue). The extension is measured at the apex of the curve, corresponding to the rupture of the physisorption link between the polymer linker and the tip. The WLC model is then fitted on the trace (dashed line) to extract the persistence length.

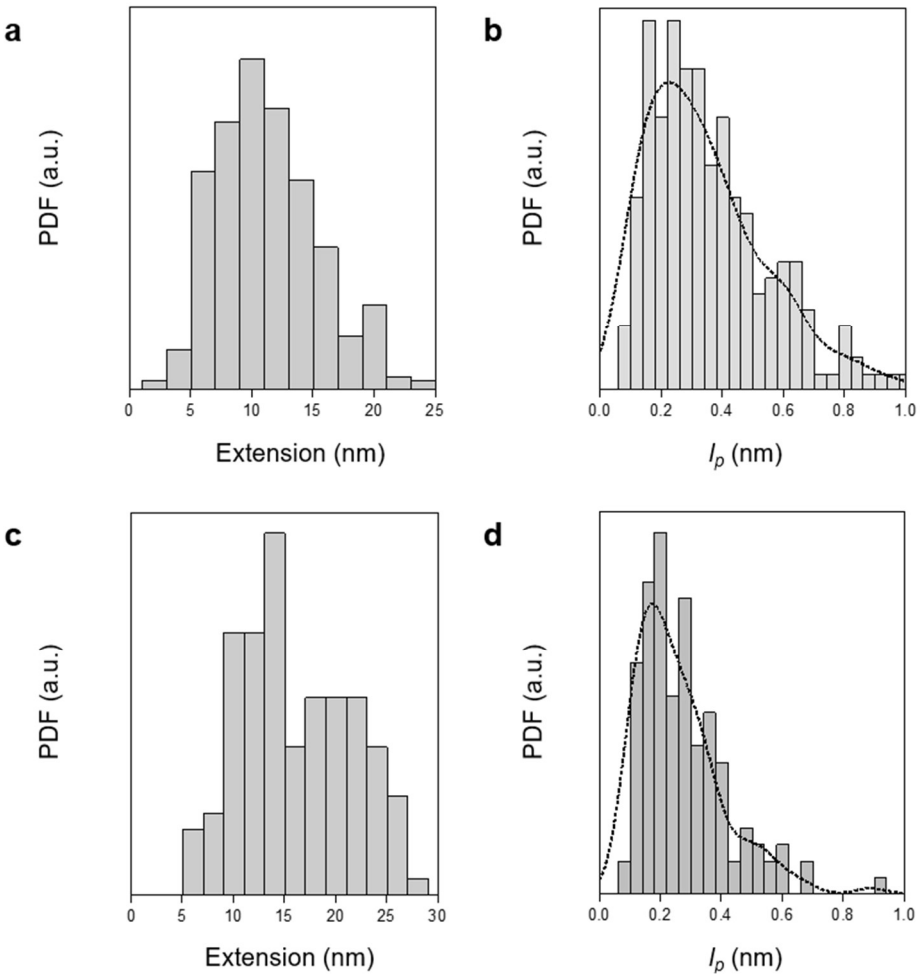

Extended Data Fig. 2: Histograms of rupture length and persistence length in approach–retraction experiments. Extension and l_p recorded at the rupture of the physisorption link between the polymer and the tip on glass surfaces (**a, b**) and on gold surfaces (**c, d**). PDF is shown as a black line.

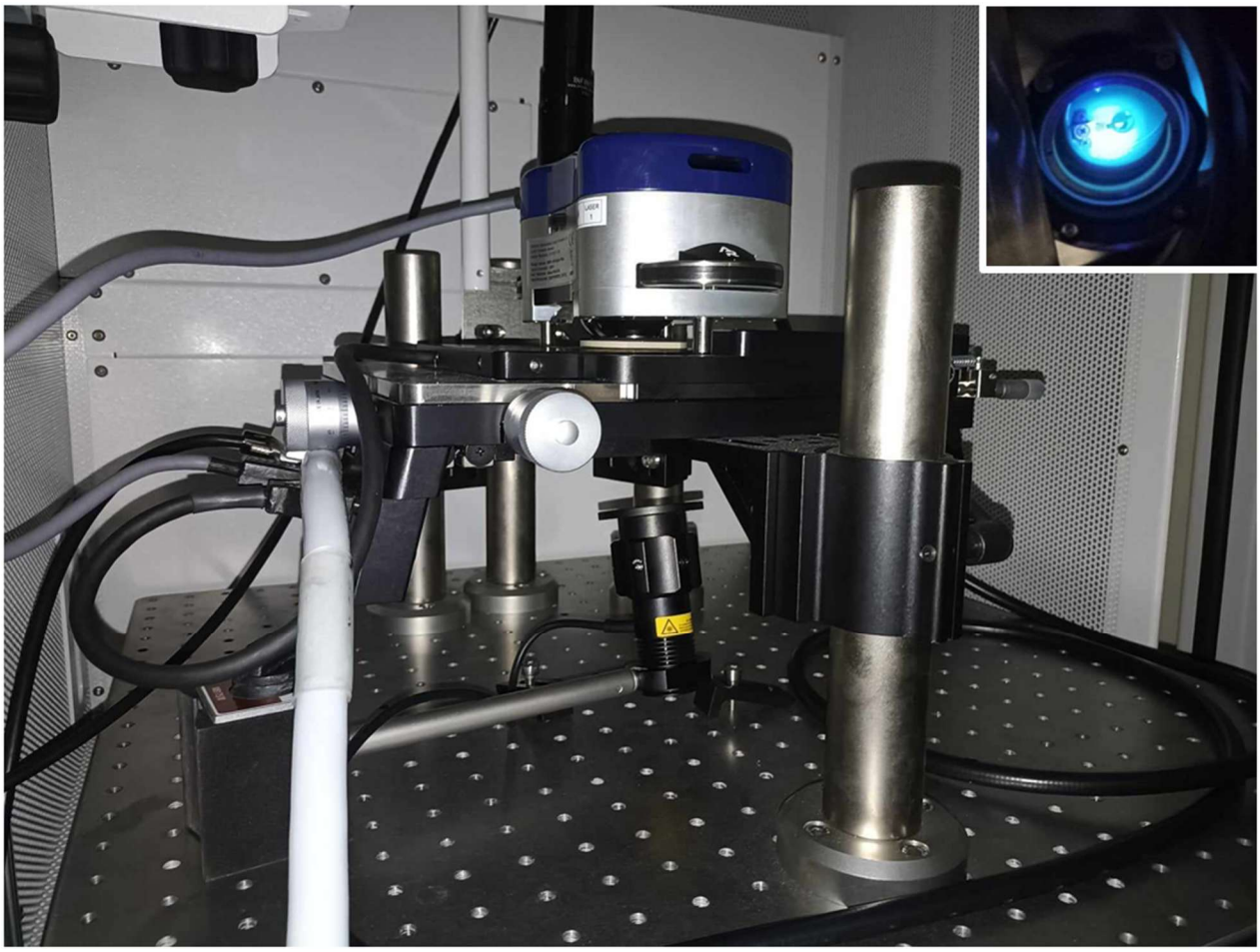

Extended Data Fig. 3: Picture of the experimental setup for the irradiation of molecular motors anchored on a glass substrate. The picture shows the lifted AFM setup which allows irradiation with a LED placed bellow the glass surface. The picture on the top right corner shows the view from the bottom: the light passes through the round glass surface where motors are grafted and reflects on the cantilever holder (blue disc).

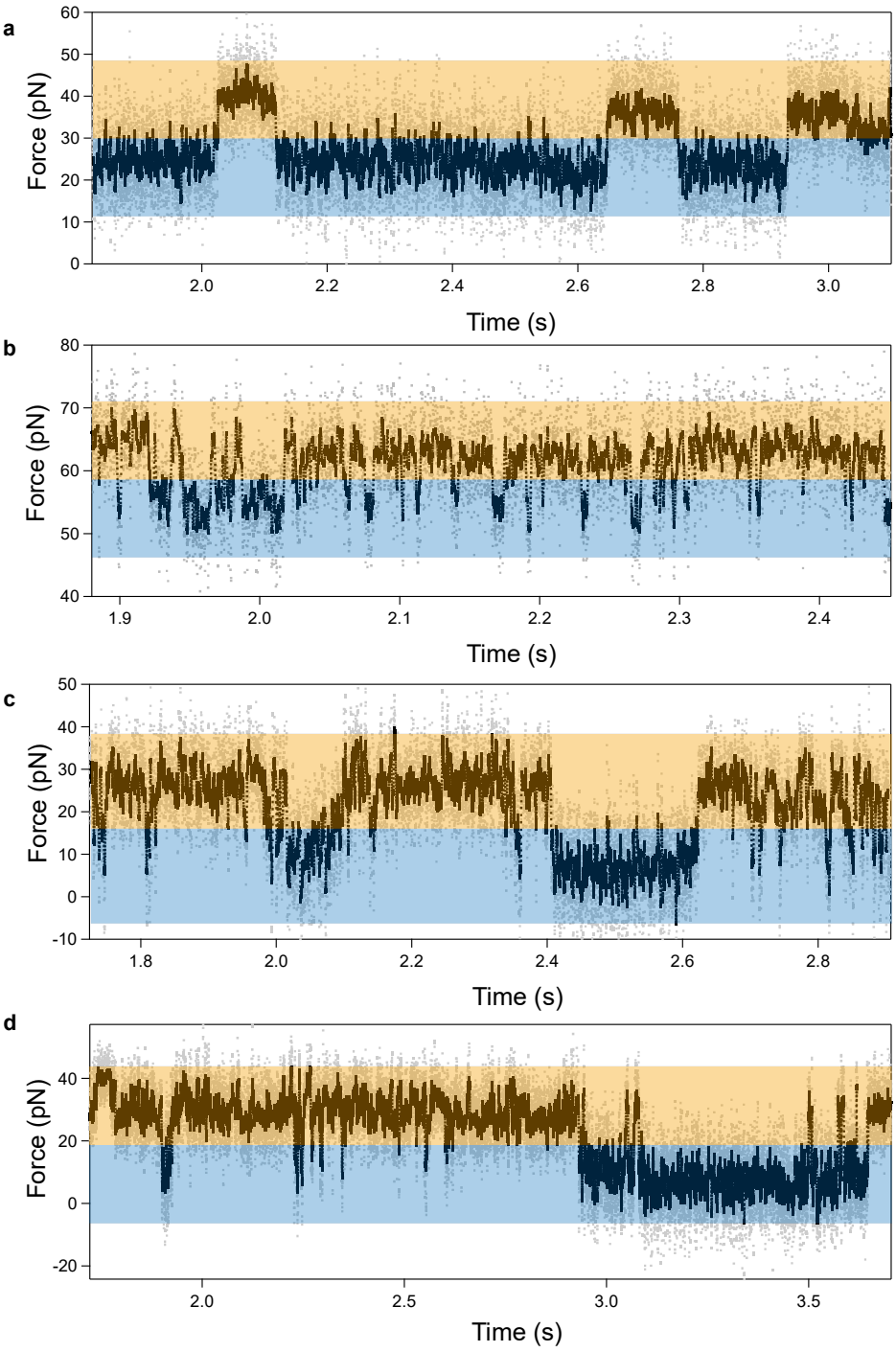

Extended Data Fig. 4: Examples of distance clamp experiments. Force versus time curves were recorded on glass (**a**, **b**) and on gold surfaces (**c**, **d**) under UV irradiation. The original data are shown as grey dots and the smoothed signal as black dots. In all cases, the hopping between two states of the motor can be seen at varying external forces and surface substrate.

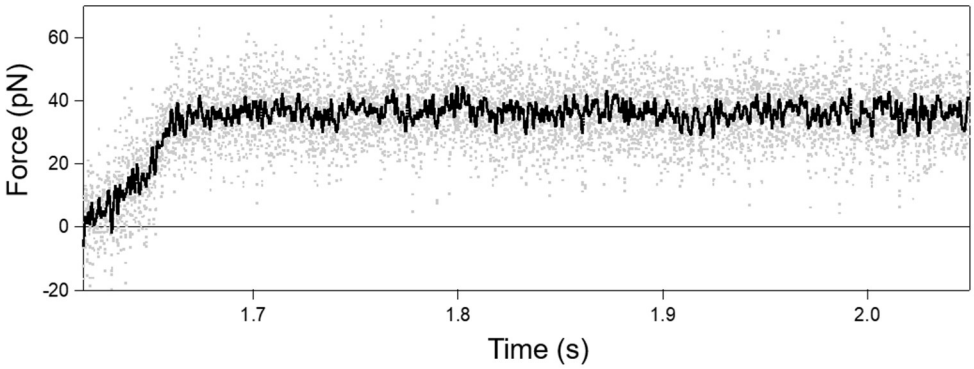

Extended Data Fig. 5: Control distance clamp experiment on motors in the dark. The polymer is first stretched to a force value of 35 pN at 1.6 seconds and kept under tension. The curve shows no hopping pattern as the motor is not irradiated with UV-light. The original data is shown as grey dots and the smoothed signal as black dots.

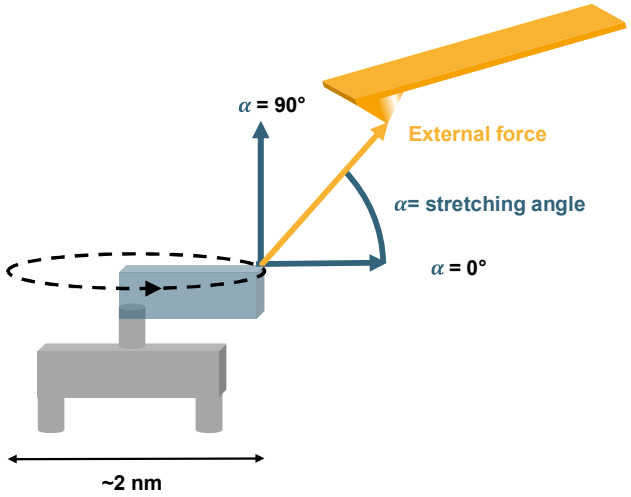

570

Extended Data Fig. 6: Schematic representation of the motor showing the external forces involved. The external force applied on the rotor by the tip can be decomposed in two components aligned with the rotation (α = 0°) and perpendicular to the rotation (α = 90°). Calculation of the value of the effective force (*i.e.* the component aligned with the rotation) is described in the methods section.

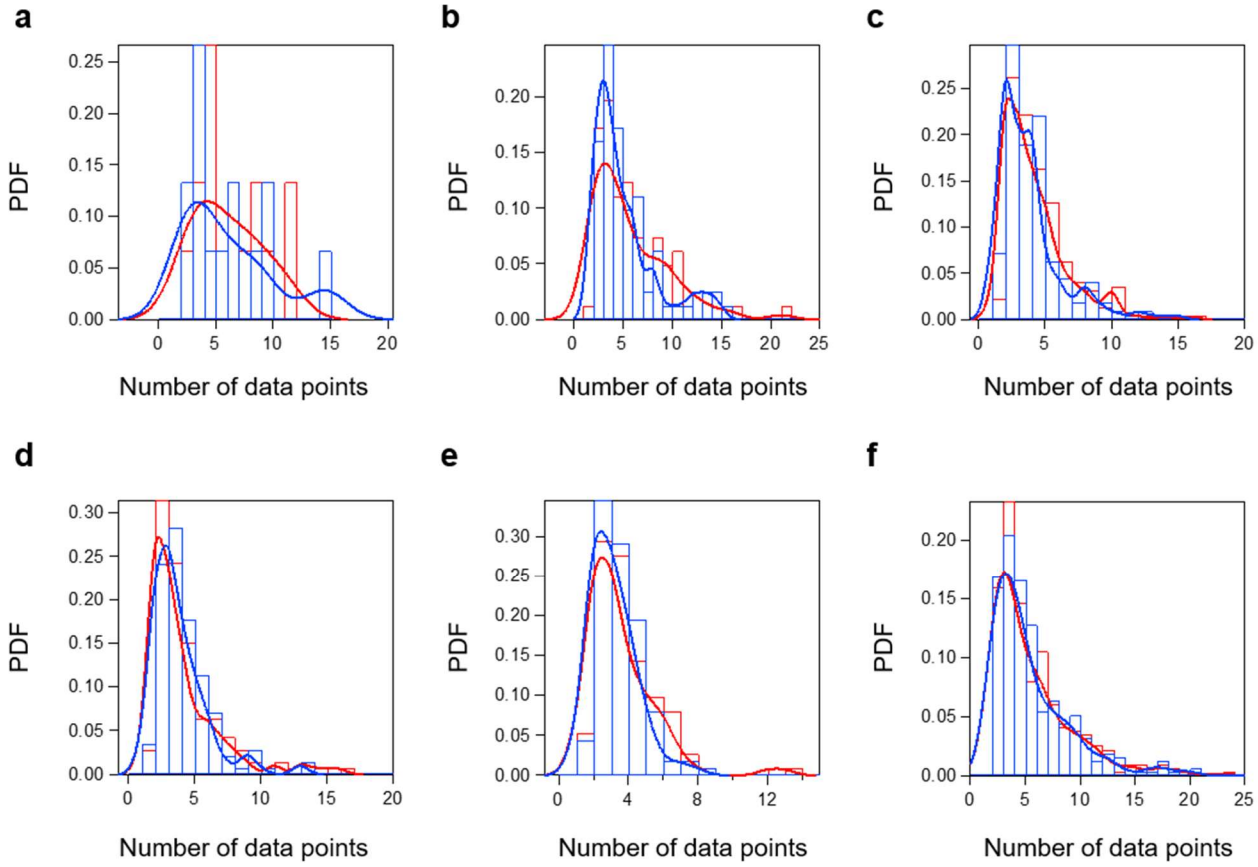

575

Extended Data Fig. 7: LTFT histograms. Histograms and associated PDF of the measured number of data points to reach the tensed state from the relaxed state (red) and reversed (blue). In all cases, histograms and PDF show a high similarity indicating equal transition times between both states.

Surface material	Force difference (pN)	Cantilever spring constant ($pN.nm^{-1}$)	Tip movement amplitude (nm)
Glass	27.36	37.6	0.73
Glass	25.21	37.6	0.67
Glass	9.54	14.2	0.67
Glass	8.39	14.8	0.57
Glass	10.04	15.7	0.64
Glass	8.23	15.7	0.52
Glass	12.47	15.7	0.79

580

Extended Data Table 1: Calculation of the amplitude of the tip movement. Force difference recorded between states and associated cantilever spring constant of each experiment used to calculated the tip movement amplitude according to Hooke's law. Obtained from 7 independent experiments.

Surface material	External Force (pN)	Effective Force (pN)
Glass	36.5	18.9
Glass	93.2	45.7
Glass	38.4	22.0
Glass	59.4	23.8
Glass	64.7	30.9
Glass	59.8	25.4
Glass	30.5	18.0
Au	19.3	14.0
Au	65.6	27.7
Au	18.5	14.8
Au	17.5	13.3

Extended Data Table 2: Effective force values. The external force can be used to calculated the effective force using the tip movement amplitude. Effective force values are shown to be independent of the surface material. The external force is the mean force value between the force value of the relaxed and tensed states. Obtained from 11 independent experiments.

Surface material	External force (pN)	PDF maximum value relaxed → tensed	PDF maximum value tensed → relax
Glass	36.46	4.1	4.4
Glass	93.21	4.3	3.5
Glass	38.38	3.2	3.1
Glass	59.36	2.1	2.3
Glass	64.65	2.3	2.8
Glass	59.80	2.5	2.4
Glass	30.52	3.1	3.2

Extended Data Table 3: External forces applied on rotor and associated with the LTFT analysis. External forces associated to the maximum value of the transition PDF. Obtained from 7 independent experiments.